PAPER Nr. : 2

AN EXPERIMENTAL INVESTIGATION OF THE INFLUENCE OF A RANGE OF AEROFOIL DESIGN FEATURES ON DYNAMIC STALL ONSET

BY

P. G. WILBY

ROYAL AIRCRAFT ESTABLISHMENT, FARNBOROUGH, UK

TENTH EUROPEAN ROTORCRAFT FORUM

AUGUST 28 – 31, 1984 – THE HAGUE, THE NETHERLANDS

AN EXPERIMENTAL INVESTIGATION OF THE INFLUENCE OF A RANGE OF AEROFOIL DESIGN FEATURES ON DYNAMIC STALL ONSET

by

P. G. Wilby

Royal Aircraft Establishment, Farnborough, UK

Abstract

Data from oscillatory pitch tests are used to evaluate the maximum value of incidence that can be attained without incurring stall during the cycle. It is deduced that, for the 12% thick aerofoils, when stall is first encountered (as mean incidence is increased) stall is triggered by a rear separation. Data from tests at constant pitch rate are then examined and it is seen that, at low pitch rates, stall is triggered by a rear separation for the thicker aerofoils. However, the rear separation is progressively suppressed as pitch rate increases, allowing a greater incidence to be attained before stall occurs, until eventually leading-edge separation provides the trigger. For an 8% thick aerofoil, stall is triggered by a leading-edge separation under all conditions.

1 Introduction

For many years there has been an interest, in the helicopter world, in the subject of dynamic stall characteristics of aerofoils because of its relevance to rotor limiting loads. Oscillatory tests on aerofoils began in the 1950s, concentrating essentially on the NACA 0012 aerofoil. Since then, several researchers have carried out detailed measurements within the boundary layer and flow field during dynamic stall, greatly adding to the fundamental understanding of the stall process. It has been shown[1,2] that dynamic stall involves the breakdown of flow at the leading edge, where a vortex forms which is transported downstream. The passage of this vortex generates large transient forces and moments and is responsible for the large nose-down pitching moment that is a feature of dynamic stall. It was later recognized[3] that this flow breakdown could be initiated by a rear separation on some aerofoils, rather than a leading-edge separation. Further studies[4,5] brought to light a flow mechanism in which flow reversal within the boundary layer can move rapidly forwards from a rear separation, leading to a leading-edge separation. It has also been noted[6] that aerofoils which exhibit a rear separation in steady conditions often display a greater stall delay in dynamic conditions than do aerofoils with a leading-edge separation. Clearly, dynamic stall is a complex phenomenon and is very important in the design of rotor blade profiles, making dynamic tests an essential part of aerofoil development. The author has previously indicated[7] that dynamic tests are needed to evaluate true steady stall incidence, and that two-dimensional dynamic tests give a realistic value for the maximum lift that can be achieved on a full scale rotor without encountering stall[8]. Thus, in recent years a series of aerofoils have been tested in dynamic conditions in support of an RAE programme on blade section research.

Although the loads generated by an aerofoil after dynamic stall onset are of great importance, the rotor designer is primarily interested in delaying the onset of stall (as much as possible). The present paper

therefore examines the recent RAE test data and attempts to draw some conclusions relating to the influence of aerofoil geometry and test conditions on stall onset.

2 Test conditions

All tests referred to in this paper were carried out by the Aircraft Research Association (ARA) at Bedford, in their aerofoil wind tunnel. This is a pressurized, intermittent blow-down facility with a working section that is 50 cm deep and 20 cm wide. Initially, tests on aerofoils in the rotor blade section research programme were conducted in steady conditions, using models of 12.5cm chord which were mounted across the full width of the tunnel. Normal force and pitching moment were calculated from measurements of chordwise pressure distributions at the centre of the models. Each test run covered only one combination of incidence and Mach number, with incidence being set prior to the run. At a later stage, ARA developed a dynamic test rig, under Ministry of Defence contract, that has been used for testing a series of aerofoils in oscillatory pitch and steady pitch rate (or ramp) conditions. For these tests, the models are again mounted across the full width of the tunnel but chord has been reduced to 10 cm. However, test Reynolds numbers of approximately $M \times 10^7$ have been possible over the Mach number range 0.3 to 0.6. Chordwise pressure distributions at the model centre line have been measured by 30 transducers mounted within the model, and provide values of normal force and pitching moment. On some models, additional pressure sensors were located at 0.075 c and 0.9 c, at 10%, 30%, 70% and 90% span as a check on the two-dimensionality of the flow. The latter have proved especially valuable at stall onset. Over the Mach number range 0.3 to 0.5 oscillatory pitch tests were made at an amplitude of $\pm 8^\circ$ at 30 Hz, and amplitude of $\pm 5^\circ$ at 30 Hz, 50 Hz and 70 Hz. For the ramp tests, pitch rates of up to 1500 deg/s were attained.

No incidence corrections have been applied to the data, but it should be noted that, in steady conditions, corrections would reduce the value of incidence by approximately 0.5° at typical stall incidence.

3 The need for dynamic tests to assess steady stall incidence

The dynamic test rig was of course developed to study dynamic stall characteristics, but it was quickly realized that it was possible to deduce the steady stall incidence from dynamic tests and that steady tests were inadequate for this purpose. Further evidence in support of these conclusions will be presented here using data for the RAE 9645 and RAE 9647 aerofoils (Fig 1) which have thickness-to-chord ratios of approximately 0.12. These aerofoils differ in rear camber, which affects the value of pitching-moment coefficient at zero lift, C_{m_0}, and in forward upper surface profile which influences the suction peak at high angles of incidence.

Steady tests at Mach numbers of 0.3 and 0.4 provided the values of normal force coefficient, C_N, and pitching-moment coefficient, C_m, which are plotted against incidence α in Fig 2. The break in C_m variation indicates stall at approximately 15° incidence at M = 0.3 and 13.5° at M = 0.4. Figs 3 and 4 show the variation of C_m with α measured

during oscillatory pitch cycles at a frequency of 2 Hz, which is too low for any significant unsteady effects to be present. These tests are referred to as quasi-steady as they can be thought of as providing steady data in a continuous running wind tunnel, where incidence is progressively increased during the run. Data for complete cycles is not shown, as the interest lies only in the region of stall at positive $\dot{\alpha}$, but results from five consecutive cycles are presented.

The first point to note in Figs 3 and 4 is that for both aerofoils at both values of M there are considerable differences between cycles, with a variation in stall incidence (as indicated by C_m break) of up to $\pm 1^o$. The second point is that C_m divergence occurs at a different angle of incidence from that for steady tests, with the difference in some cases being greater than 2^o. Thirdly, it is seen that the difference between steady and quasi-steady stall angle is much larger for the RAE 9647 profile than for RAE 9645. These results will now be compared with the values of stall incidence deduced from dynamic tests, following the procedure given in Ref 7.

The variation of C_N and C_m with α is shown in Figs 5 and 6 for the two aerofoils at M = 0.3 during oscillatory pitch cycles with amplitude of $\pm 8^o$ and frequency of 30 Hz. This gives a reduced frequency $k = \pi fc/v$ that corresponds to a once per revolution variation on a typical full scale rotor. The mean incidence for these cycles is progressively increased, taking the aerofoils from unstalled conditions on the left to well stalled conditions on the right of the figures. The deviation in C_m, marked as ΔC_m in the figures, is plotted in Fig 7 against the maximum value of α achieved during the cycle, and the intercept with $\Delta C_m = 0$ gives the critical value of incidence α_c. It was argued in Ref 7 that α_c could be taken as the steady stall incidence and this will be assumed to be valid here, although recent evidence suggests that in some cases there are variations in α_c depending upon frequency and amplitude combinations. The deduced values of stall incidence are shown in Fig 8 compared with those measured in steady and quasi-steady conditions. Considerable differences are found between the different types of test, and different patterns of these variations are exhibited by the two aerofoils.

Some of the factors that lead to different values of stall incidence being given by different types of test must now be considered. In the quasi-steady tests, stall incidence is approached from low incidence, unstalled conditions after the tunnel speed has been established. However, in the steady tests the incidence is set before the tunnel flow accelerates from zero to the desired speed, which means that at high angles of incidence the initial flow is likely to be separated, with attachment occurring as Reynolds number increases during the establishment of steady test conditions. Eventually, at some angle of incidence, the flow will fail to attach at the test conditions. Thus the approach to stalled conditions is more akin to the downstroke of the quasi-steady tests in which attached flow is approached from separated conditions. In fact, the stall incidence obtained in steady tests is much closer to the quasi-steady attachment incidence than it is to the stall incidence. This is of course the familiar hysteresis effect of steady two-dimensional testing.

A further factor was noted in the quasi-steady tests for the RAE 9647 aerofoil. This was the strong spanwise variation in pressure measured at 7.5% and 90% chord that appeared as stall was approached, indicating flow separation at the model/wall junction. Such a separation would give rise to a trailing vortex at each end of the model which would reduce the effective angle of incidence over the centre of the model. In these circumstances the model attitude would no longer be the true aerodynamic incidence. At the higher frequencies of the true dynamic tests it was found that the spanwise distribution of pressure was much more uniform at stall onset, indicating that the end separation was suppressed, giving conditions much closer to true two-dimensional flow. On these arguments, dynamic tests are more likely to give an accurate measure of stall incidence than are steady or quasi-steady tests.

For aerofoils intended for use on helicopter rotor blades it is the difference between stall incidence and zero-lift incidence α_0 that is important. Assuming that stall incidence can be represented by α_c as obtained from dynamic tests, the value of $\alpha_c - \alpha_0$ is plotted against M in Fig 9 for RAE 9645, RAE 9647 and NACA 0012. It is seen that the RAE 9645 profile provides a gain over NACA 0012 in this quantity of about 30% at $M = 0.35$.

4 The influence of leading edge and rear profiles on stall onset in oscillatory pitch conditions

In the following analysis of experimental results attention will focus on the value of critical incidence α_c as defined in the previous section, as this is the maximum incidence that can be attained during an oscillatory pitch cycle without stall occurring. Stall can of course be delayed to a higher value of incidence than α_c provided the value of pitch rate $\dot{\alpha}$ is high enough, as has already been seen in Figs 5 and 6, but stall cannot be avoided once α_c has been exceeded.

Referring to the dynamic test results shown in Fig 7, it is noted that at $M = 0.3$ the stall incidence, or α_c, is the same for both RAE 9645 and RAE 9647 aerofoils. This is in spite of the fact that the RAE 9647 aerofoil has a much more severe adverse pressure gradient aft of the leading-edge section peak, as seen in Fig 10. The pressure distributions shown in Fig 10 were obtained during the up-stroke of the second cycle from the left shown in Figs 5 and 6. This suggests that, at this particular combination of amplitude and frequency, leading-edge pressure distribution is not the dominant factor for stall for these two aerofoils, and that perhaps stall is triggered by a rear separation.

Test results for the RAE 9648 aerofoil (Fig 11) are useful in considering the possible role of rear separation. This aerofoil has a concavity on the rear upper surface to give reflex camber and a positive value of C_{m_0}. The effect on the upper surface pressure distribution is to give a steeper adverse gradient, when compared with RAE 9645, in the region of 70% chord. The two aerofoils have identical nose profiles and can be expected to have similar leading-edge pressure distributions, although the

suction peak at a given value of incidence should be rather less on RAE 9648 because of the reduced circulation. The oscillatory pitch test data presented in Fig 12 shows that the RAE 9648 aerofoil stalls at a lower value of incidence than RAE 9645. As the leading-edge pressure gradient must be slightly less severe for RAE 9648, stall must be triggered by a rear separation which is aggravated by the more severe rear pressure gradient. The lower value of α_c, coupled with a higher value of α_0 due to the reflex camber, gives a greatly reduced value of $\alpha_c - \alpha_0$ as seen in Fig 13.

Further data from the oscillatory pitch cycles shown in Figs 14 and 15 support the above arguments. Fig 14 plots the variation of pressure coefficient C_p at 0.5% chord during two cycles of incidence and shown the lower suction peak for the RAE 9648 profile. The variation of C_m with α for the same two cycles is shown in Fig 15, where the drop in C_m at the beginning of the downstroke for the left-hand cycle for RAE 9648 suggests the local increase in rear loading that would accompany a local rear separation with re-attachment. In the right-hand cycle, during which a higher angle of incidence is attained, stall develops completely, leading to a large nose-down pitching moment. Such a large drop in C_m is usually attributed to the passage over the upper surface of a vortex formed when the boundary layer separates at the leading edge. The implication then must be that a disturbance has been transmitted upstream through the boundary layer from the rear separation, leading to a breakdown in leading-edge flow, following one of the mechanisms described in Refs 3 and 4.

Returning to the influence of leading-edge pressure distribution on stall onset, the RAE 9681 aerofoil was designed as a modification to the RAE 9647 profile (Fig 16) to give a reduced leading-edge suction peak (Fig 17). Results from oscillatory pitch tests for an amplitude of $\pm 8^o$ at a frequency of 30 Hz show little effect on α_c (Fig 18), providing further support for the idea that stall is triggered by a rear separation. The fact that the rate of increase in the magnitude of ΔC_m with maximum incidence is less for the modified aerofoil at M = 0.3 may be due to a leading-edge pressure gradient that is less sensitive to the disturbances moving upstream in the boundary layer.

5 Effect of Reynolds number

During the test programme on the RAE 9681 aerofoil the opportunity was taken of obtaining some measurements at M = 0.3 at the lowest possible Reynolds number, which is close to the value appropriate to model rotor tests. The aim was to determine whether or not dynamic stall would occur at a lower value of incidence on model rotors than on full-scale rotors. Fig 19 gives the measured variation of C_m with α for three cycles of amplitude $\pm 8^o$ and frequency 30 Hz, with progressively increasing mean incidence, for Reynolds numbers of 2.7 and 1.15×10^6. Comparing results for the third cycle at the higher Reynolds number with the second cycle at the lower Reynolds number, it is seen that the stall incidence is

reduced by about 1.5° by the drop in Reynolds number. Clearly, on this basis, one should expect to see a marked difference in dynamic stall onset between model rotor and full-scale tests.

6 Characteristics of a thick aerofoil

The use of thick aerofoil sections over the inner part of rotor blades offers considerable structural benefits, and thick sections have therefore been studied as part of the RAE programme.

One of these is the 16% thick RAE 9651 aerofoil, shown in Fig 20 in comparison with the RAE 9645 profile. It is seen that the two aerofoils have identical upper surfaces except at the extreme leading edge where the RAE 9651 section has a much larger radius. The extra thickness was applied to the lower surface so as not to steepen the rear pressure gradient on the upper surface which already provides the trigger for stall on RAE 9645. Again, test results for an amplitude of $\pm 8^{\circ}$ and frequency of 30 Hz are presented in Fig 21 where it is seen (on comparing with Fig 7) that α_c is appreciably higher than for RAE 9645.

This is rather an unexpected result as one might anticipate that, if stall is triggered by a rear separation and the two aerofoils have essentially similar rear pressure gradients, stall will occur at the same angle of incidence. There will however be some differences in the pressure distribution due to the appreciable differences in circulation for the two aerofoils (α_0 is 0.5° for RAE 9651 but -2° for RAE 9645). There could also be some secondary effects of the considerable reduction in leading-edge suction peak on RAE 9651 which may influence the state of the rear boundary layer such that it can tolerate a more severe pressure gradient before separating.

In terms of effective incidence, the increase in α_c for RAE 9651 is offset by the increase in α_0, and the value of $\alpha_c - \alpha_0$ (Fig 22) is a little below that for RAE 9645. However, this is still a very good result for such a thick section, especially when it is remembered that the thick section has an appreciable amount of reflex camber to give a positive value of C_{m_0}.

7 Characteristics of a thin aerofoil

At high forward speed there are benefits, in terms of drag reduction, in having a thin section at the advancing blade tip. However, such a section must retain a reasonably high stall incidence at low values of Mach number if it is to operate effectively on the retreating side of the disc. Attention was therefore turned to sections of approximately 8% thickness-to-chord ratio, one of which is the RAE 9634 aerofoil shown in Fig 23. The C_m variation during pitch cycles of $\pm 8^{\circ}$ amplitude and frequency of 30 Hz is shown in Fig 24, and the deduced value of α_c is used to give the values of $\alpha_c - \alpha_0$ plotted in Fig 25 against Mach number. It is seen that over the Mach number range 0.3 to 0.5 the thin aerofoil

has a marginally higher effective stall angle than NACA 0012. The RAE 9634 aerofoil has of course a much higher drag-rise Mach number than NACA 0012.

In terms of features that trigger stall, little can be deduced from these tests alone but more can be learnt from the ramp test results to be discussed in the next section.

8 Stall onset in steady pitch motion

In addition to oscillatory pitching motion, the ARA dynamic rig can also give a steady rate of pitch (or ramp type variation of incidence with time) which has proved to be very useful in the investigation of dynamic stall. Some results from the ramp tests for RAE 9645 are given in Fig 26, for M = 0.3, where pressure coefficient at 0.5% chord and C_m are plotted against incidence for four values of pitch rate $\dot{\alpha}$. It is seen that, as pitch rate increaes, the aerofoil reaches progressively higher angles of incidence before stall occurs (stall being indicated by the C_m break or the rapid drop in leading-edge suction). Furthermore, it is found that the suction peak at stall (as indicated by C_p at 0.5% chord) gets progressively higher as stall incidence increases. This suggests that the suction peak does not itself trigger stall. However, once the pitch rate reaches 1200 deg/s the suction peak no longer increases with increased pitch rate and there is little significant change in stall incidence. A possible interpretation of the data is that at low pitch rates stall is triggered by a rear separation which is progressively suppressed as pitch rate increases. This allows greater values of incidence, and higher suction peaks, to be attained before stall occurs. At high pitch rates the rear separation is sufficiently suppressed for the leading-edge pressure distribution to become the stall trigger. Beyond this stage, an increase in pitch rate will not further suppress separation.

A similar picture is depicted in Fig 27 for the RAE 9648 aerofoil but, as one would expect from the oscillatory tests, stall incidence is lower than for RAE 9645 at low pitch rates due to the more severe rear pressure gradient. In Fig 28 the value of incidence corresponding to the minimum value of C_p at 0.5% chord (a much better defined criterion for stall than C_m break) is plotted against pitch rate. This shows the lower stall incidence for RAE 9648 at low values of $\dot{\alpha}$, and the convergence of stall incidence for the two aerofoils as pitch rate increases and stall becomes dependent on leading-edge pressures.

The RAE 9681 aerofoil was tested at only two values of pitch rate, but results shown in Fig 29 follow the pattern described above, with suction peak at stall increasing in magnitude as increasing pitch rate delays separation.

In Fig 30 we see the same overall trends for the thicker RAE 9651 aerofoil, but with some underlying differences. Compared with RAE 9645 (Fig 26) the higher angle of stall incidence observed in oscillatory tests is again exhibited, but stall is a much more gradual process, and at low values of pitch rate there are signs of an initial rear separation which does not develop into full stall until a much higher angle of incidence is attained. One possibility is that, as this aerofoil has a very much lower

suction peak at the leading edge than RAE 9645, it is more difficult for boundary-layer disturbances, travelling forwards from the rear separation, to precipitate a leading-edge stall.

A different progression of events is found in Fig 31 for the thin RAE 9634 aerofoil. Here, there is very little change in minimum pressure over a considerable range of pitch rate. However, the suction peak reaches a much higher level at low pitch rates than on the thicker aerofoils, and is already close to the limiting value for those aerofoils. This suggests that the RAE 9634 section is thin enough to avoid a rear separation and, even at low pitch rates, stall is triggered by a leading-edge separation.

9 Discussion

It is useful first of all to compare the values of pitch rate that were encountered in the oscillatory pitch tests with those of the steady pitch-rate tests. Fig 32 plots pitch rate against incidence for a sinusoidal oscillation of $\pm 8^{\circ}$ amplitude about zero degrees mean incidence at a frequency of 30 Hz. It is seen that the pitch rate reaches a maximum of 1500 deg/s which is the maximum value attained in the steady pitch-rate tests.

Referring to the cycle in Fig 32, let us now consider the importance of operating conditions by taking the example of the RAE 9645 aerofoil. It has been deduced that a rear separation on RAE 9645 is fully suppressed when pitch rate reaches or exceeds 1200 deg/s. This means that, for the cycle represented in Fig 32, a rear separation would be fully suppressed during the up-stroke over the incidence range -5° to 5° (noting that $\dot{\alpha} = 1200$ deg/s at $\alpha = \pm 5^{\circ}$). It has further been deduced that, with a fully suppressed rear separation, leading-edge stall will occur at $\alpha = 20^{\circ}$ when $\dot{\alpha} = 1200$ deg/s . Thus, if mean incidence were set at 15° then $\dot{\alpha}$ would fall to the critical value of 1200 deg/s at $\alpha = 20^{\circ}$ and we would expect to see a leading-edge stall occur at that point. Incidence at stall onset would be 3° below the maximum value attained during the cycle.

Following similar arguments, if frequency were doubled (and pitch rate doubled) then, for a mean incidence of 12.5°, leading-edge stall would occur at only 0.5° below the maximum value of incidence. These arguments demonstrate that stall is not confined to the rear separation type in oscillatory pitch conditions, and all factors must be accounted for in assessing rotor blade stall onset. As was pointed out earlier, the frequency of 30 Hz for the model aerofoil gives a reduced frequency that corresponds to a once per revolution variation for a full-scale rotor. However, the pitch rate on the retreating side of the disc could be much higher than for a once per revolution variation due to local effects of tip vortices. Clearly it is important to understand fully the rotor blade operating conditions before drawing full benefit from the data analysis that has been presented here. Once these conditions are established it may be possible to define an optimum combination of suction peak and rear pressure gradient to allow the highest possible angle of incidence to be attained without stall occurring. This would imply some optimum combination of camber and thickness distribution.

10 Conclusions

The main conclusions to be drawn from the analysis of experimental data that has been presented here are as follows.

(a) Steady aerofoil tests are unreliable for the measurement of steady stall incidence, which can however be deduced from dynamic tests.

(b) Cambered aerofoils of 12% thickness are likely to exhibit dynamic stall triggered by a rear separation under certain oscillatory pitch conditions and at low pitch rates. As pitch rate increases, the rear separation is progressively suppressed until leading-edge separation becomes the stall trigger.

(c) 16% thick aerofoils can be designed without penalty of lower stall incidence relative to 12% thick sections.

(d) Dynamic stall for thin aerofoils is likely to be triggered by a leading-edge separation under all conditions.

(e) A full understanding of rotor blade operating conditions (in terms of incidence and pitch rate variations) is needed before the optimum combination of leading-edge suction peak and rear pressure gradient can be defined in order to give the highest possible incidence that can be achieved without inducing stall.

References

1 W. Johnson and N.D. Ham, On the mechanism of dynamic stall, *J. of Am. Helicopter Society*, Vol 17, No.4, October 1972.

2 P. Crimi and B.L. Reeves, A method for analyzing dynamic stall, *NASA CR-2009*, May 1972.

3 W.J. McCroskey and J.J. Philippe, Unsteady viscous flow on oscillating airfoils, *AIAA Paper No.74-182*, Washington DC, January 1974.

4 W.J. McCroskey, L.W. Carr and K.W. McAlister, Dynamic stall experiments on oscillating airfoils, *AIAA Paper No.74-125*, Pasadena, California, January 1975.

5 L.W. Carr, K.W. McAlister and W.J. McCroskey, Analysis of the development of dynamic stall based on oscillating airfoil experiments, *NASA TN D-8382*, January 1977.

6 T.S. Beddoes, Onset of leading-edge separation effects under dynamic conditions and low Mach numbers, *34th Annual Nation Forum of the AHS*, Washington DC, May 1978.

7 P.G. Wilby, The aerodynamic characteristics of some new RAE blade sections, and their potential influence on rotor performance, *Vertica*, Vol 4, pp 121-133, 1980.

8 P.G. Wilby, M.J. Riley and Judith Miller, Some unsteady aerodynamic effects on helicopter rotors, *7th European Rotorcraft Forum*, Garmisch-Partenkirchen, September 1981.

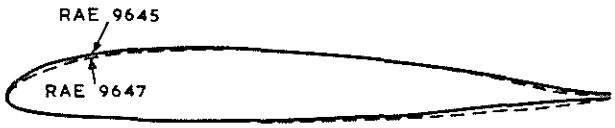

Fig 1 Aerofoil profiles

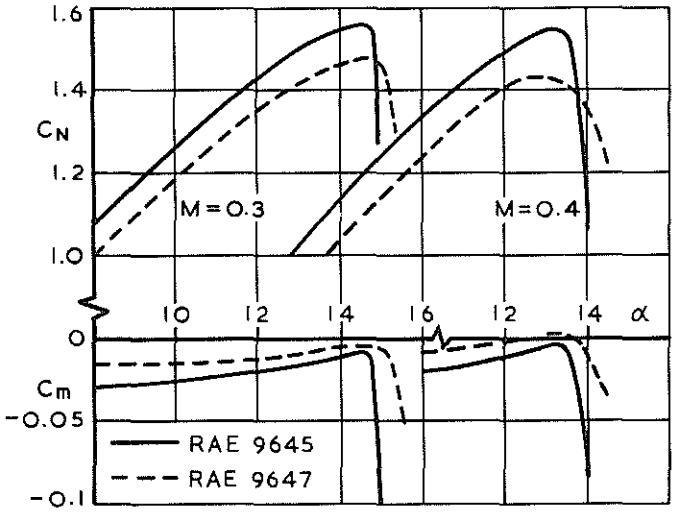

Fig 2 Steady test data as an indication of stall

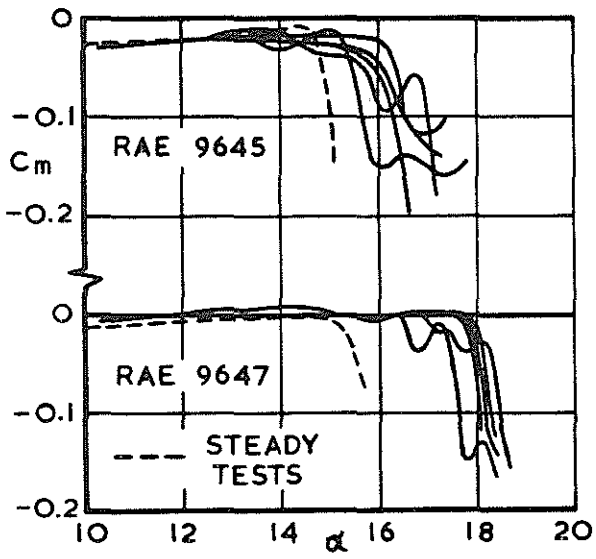

Fig 3 Pitching-moment break in quasi-steady incidence variation at M = 0.3

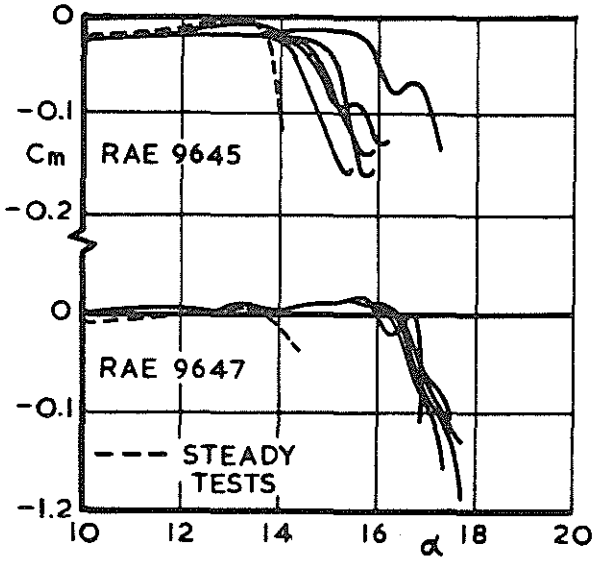

Fig 4 Pitching-moment break in quasi-steady incidence variation at M = 0.4

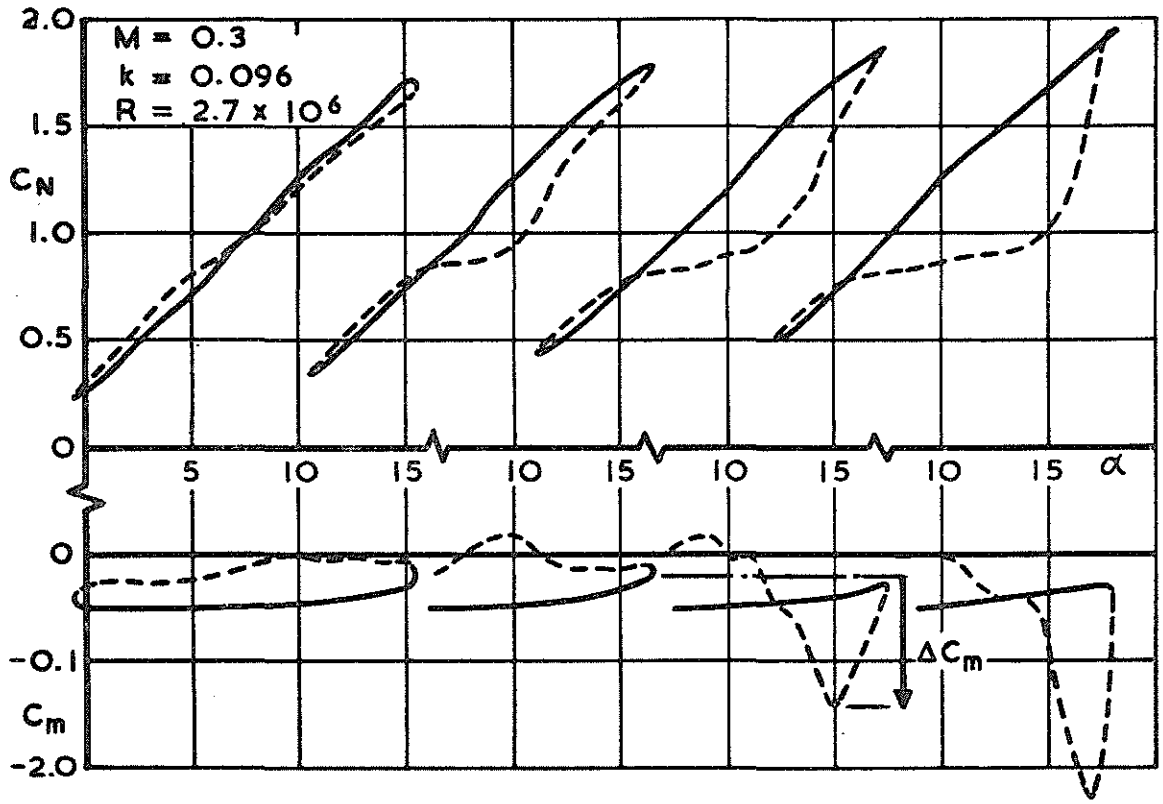

Fig 5 Variation of normal force and pitching-moment coefficient with incidence during a series of pitch cycles for RAE 9645

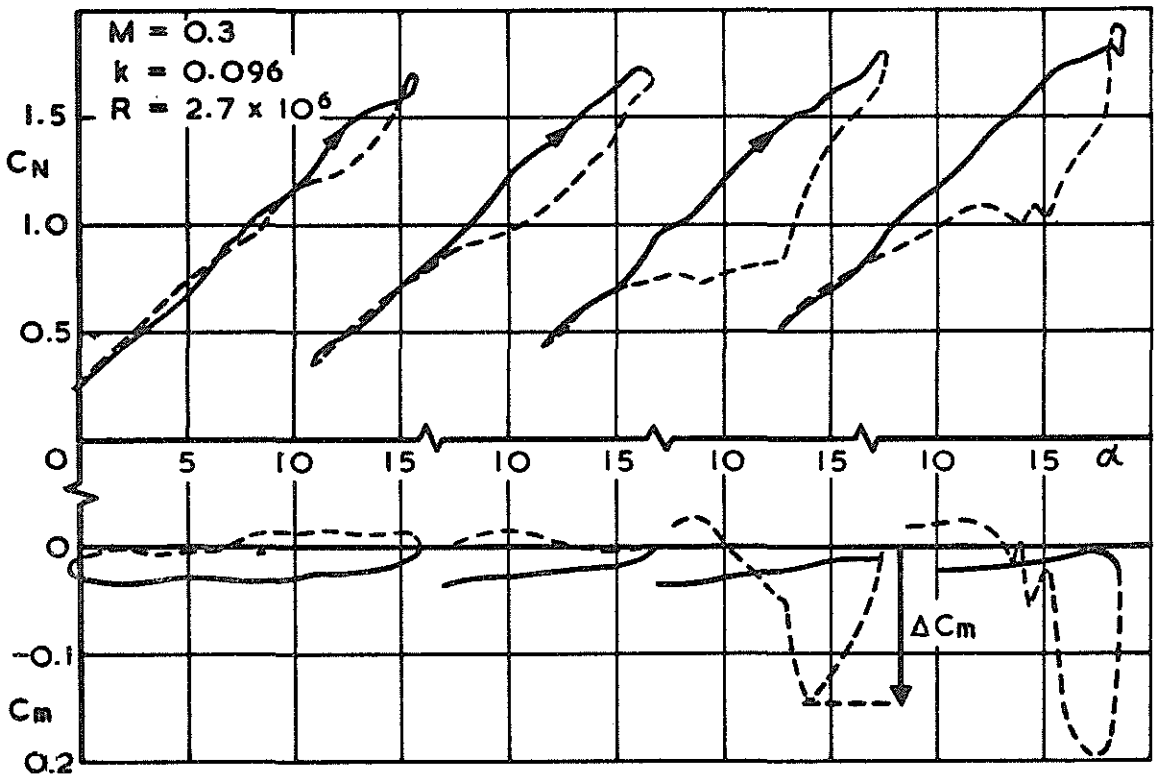

Fig 6 Variation of normal force and pitching-moment coefficient with incidence during a series of pitch cycles for RAE 9647

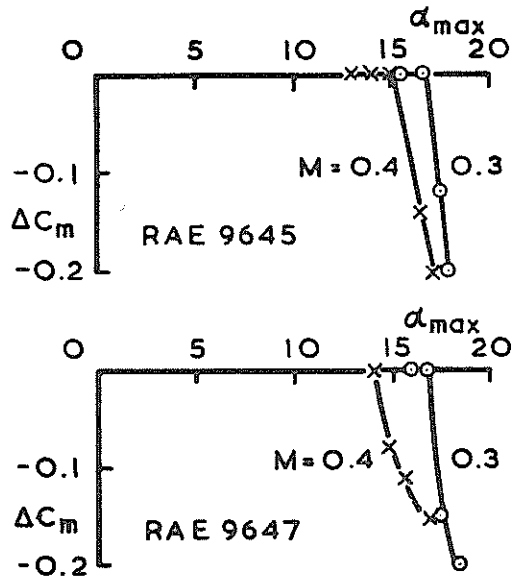

Fig 7 Pitching-moment deviation in oscillatory pitch cycles

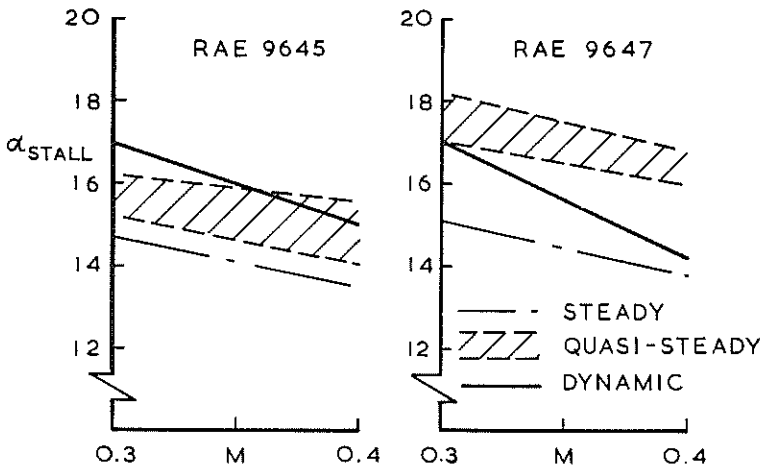

Fig 8 Stall incidence as indicated by different test conditions

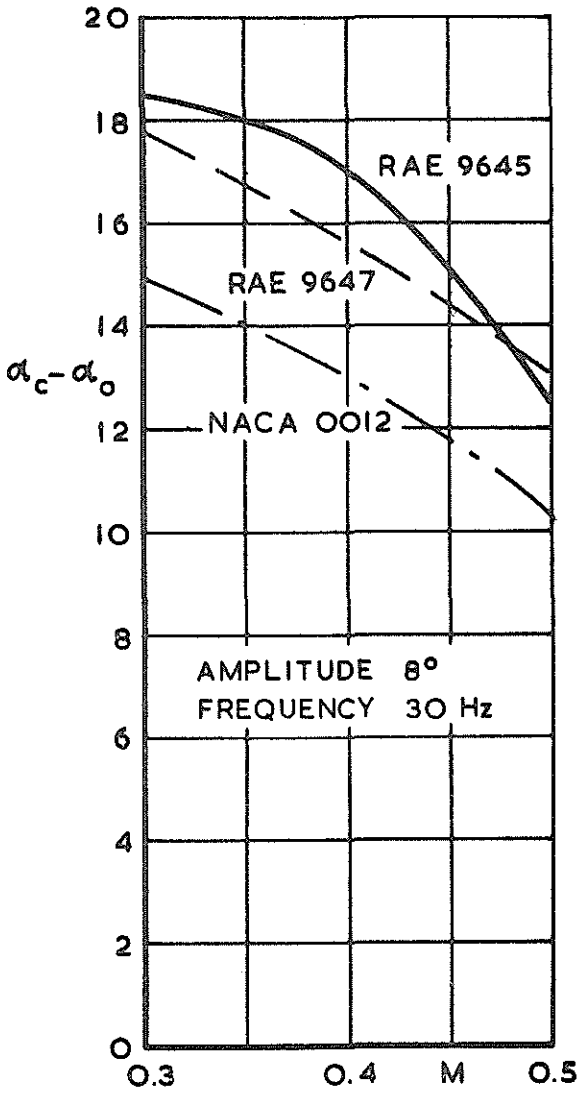

Fig 9 Maximum effective incidence attained during oscillatory pitch cycle without stalling

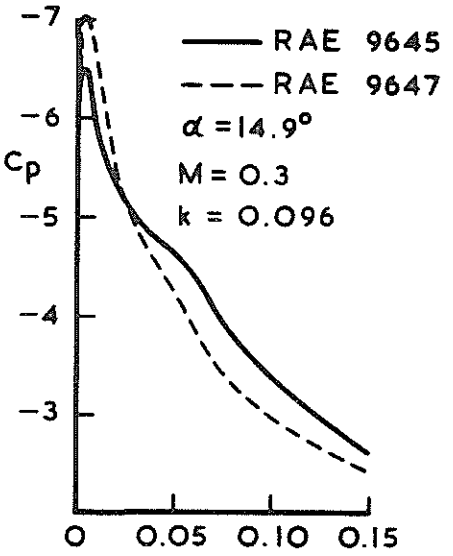

Fig 10 Leading-edge suction peak measured during oscillatory pitch cycle

Fig 11 Aerofoil profiles

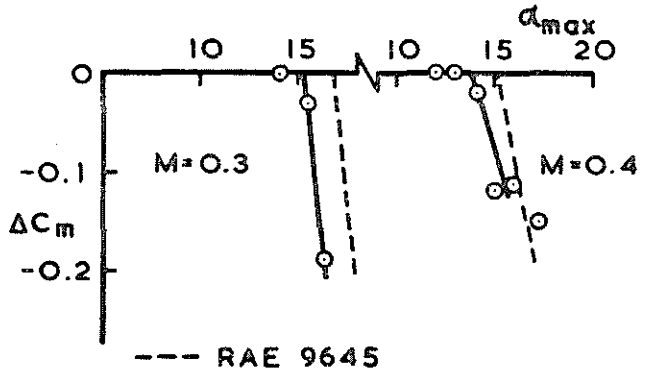

Fig 12 Pitching-moment deviation for RAE 9648

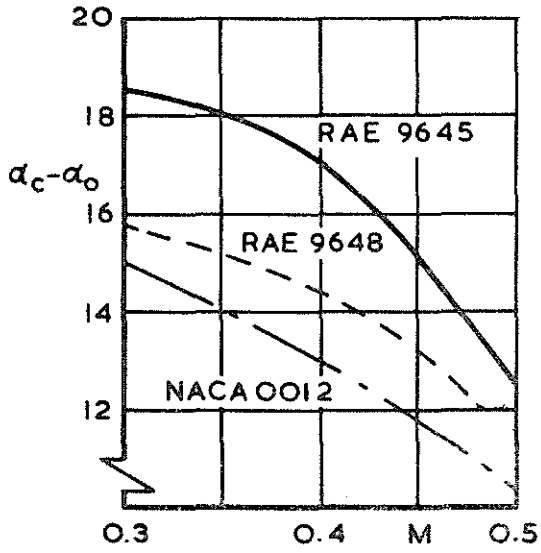

Fig 13 Maximum effective incidence attained during oscillatory pitch cycle without stalling

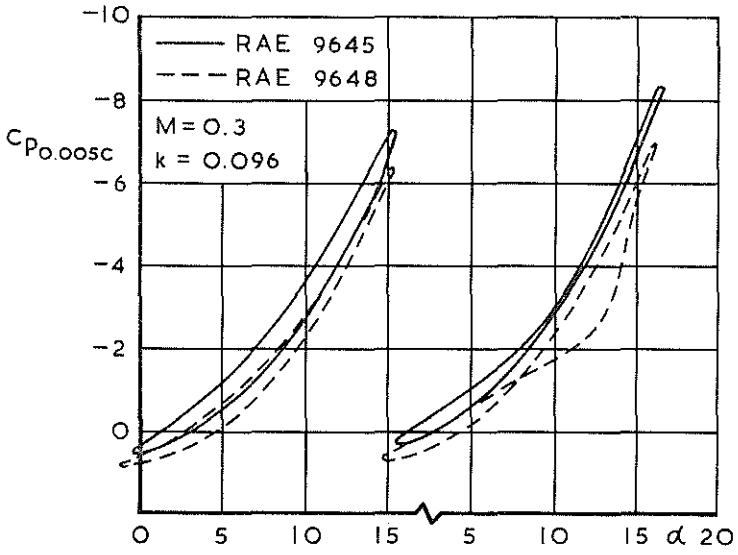

Fig 14 Variation of pressure coefficient during oscillatory pitch cycles at 0.5% chord with incidence

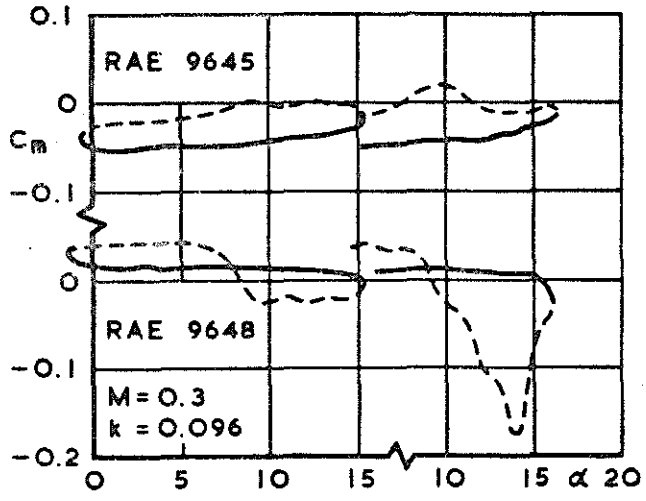

Fig 15 Variation of pitching-moment coefficient with incidence during oscillatory pitch cycles

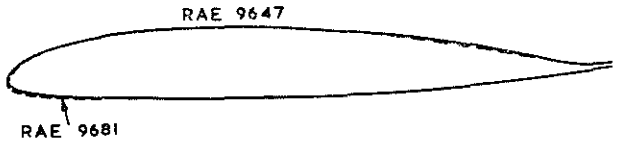

Fig 16 Aerofoil profiles

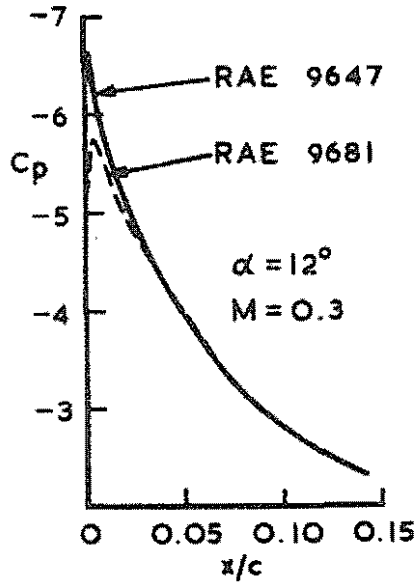

Fig 17 Theoretical inviscid leading-edge pressure distribution

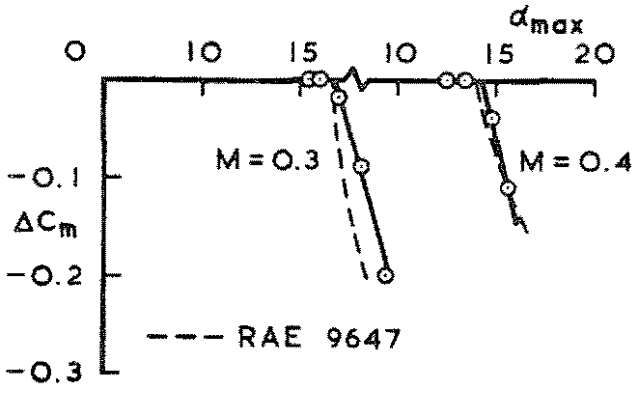

Fig 18 Pitching-moment deviation for RAE 9681

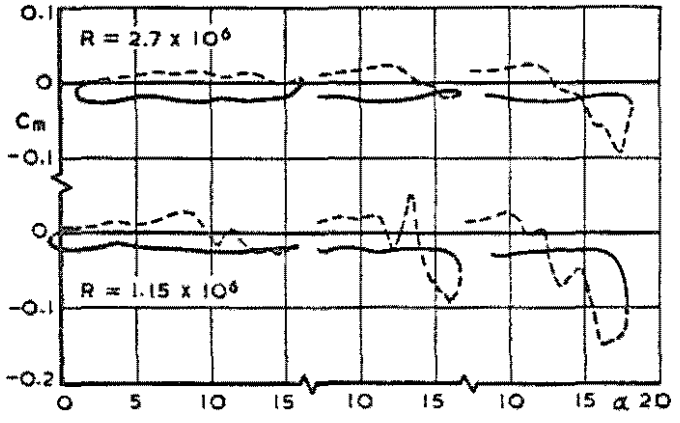

Fig 19 Effect of Reynolds number on pitching-moment break for RAE 9681 during oscillatory pitch cycles at M = 0.3

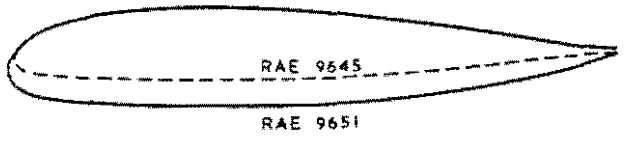

Fig 20 Aerofoil profiles

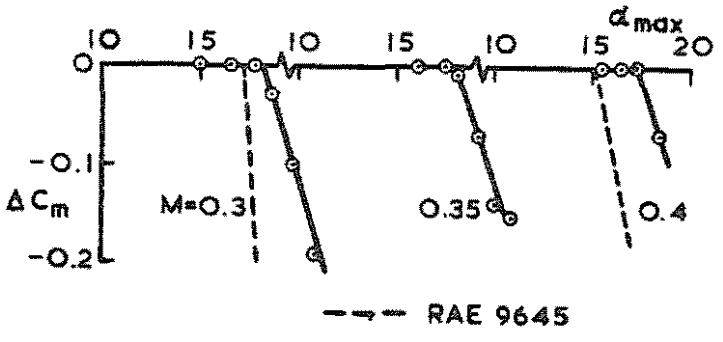

Fig 21 Pitching-moment deviation for RAE 9651

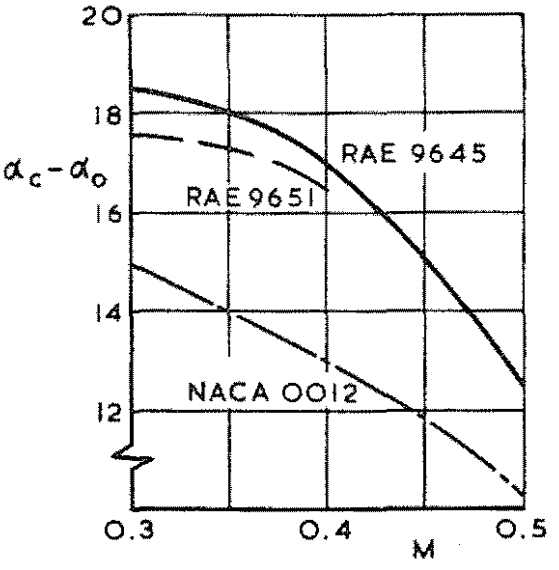

Fig 22 Maximum effective incidence attained during oscillatory pitch cycle without stalling

Fig 23 RAE 9634 profile

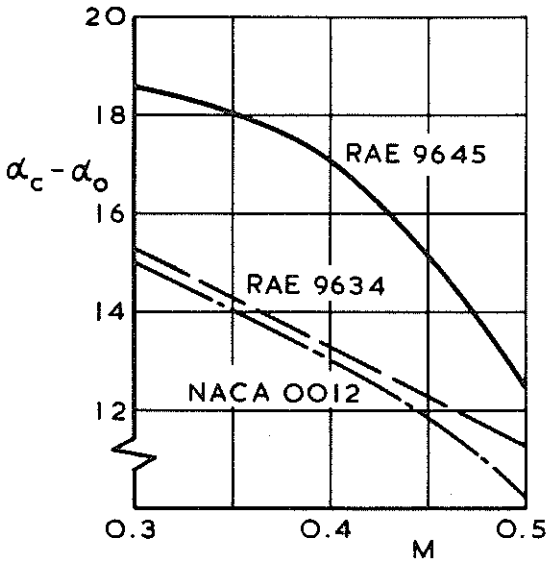

Fig 25 Maximum effective incidence attained during oscillatory pitch cycle without stalling

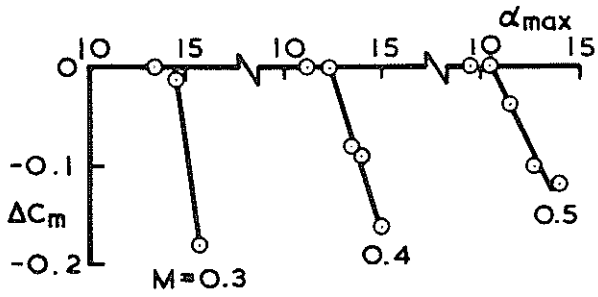

Fig 24 Pitching-moment deviation for RAE 9634

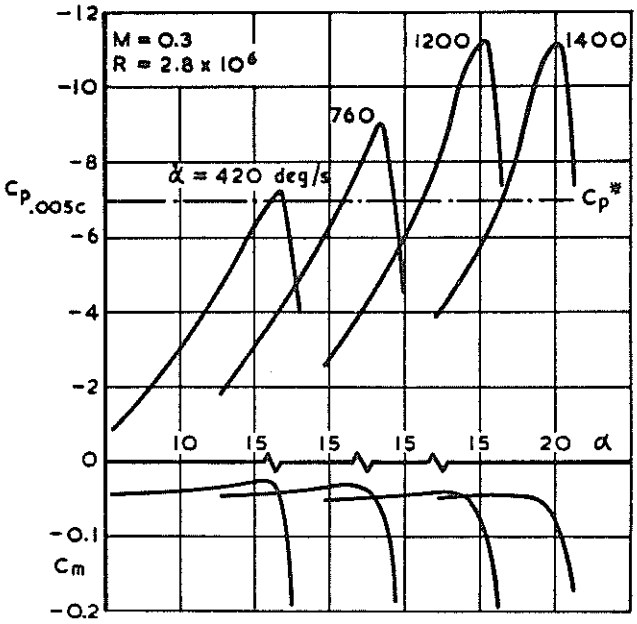

Fig 26 Variation of leading-edge pressure coefficient and pitching-moment coefficient with incidence during steady pitch rate motion for RAE 9645

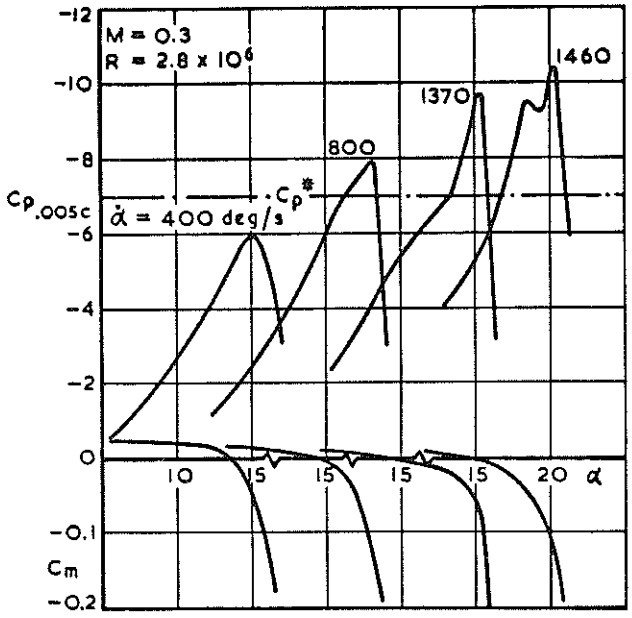

Fig 27 Variation of leading-edge pressure coefficient and pitching-moment coefficient with incidence during steady pitch rate motion for RAE 9648

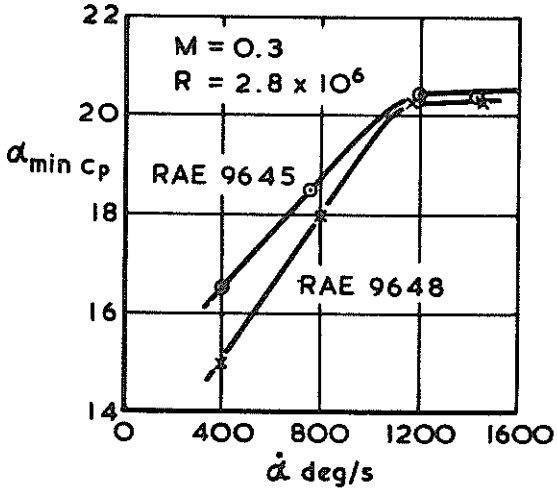

Fig 28 Incidence for minimum C_p as a function of pitch rate

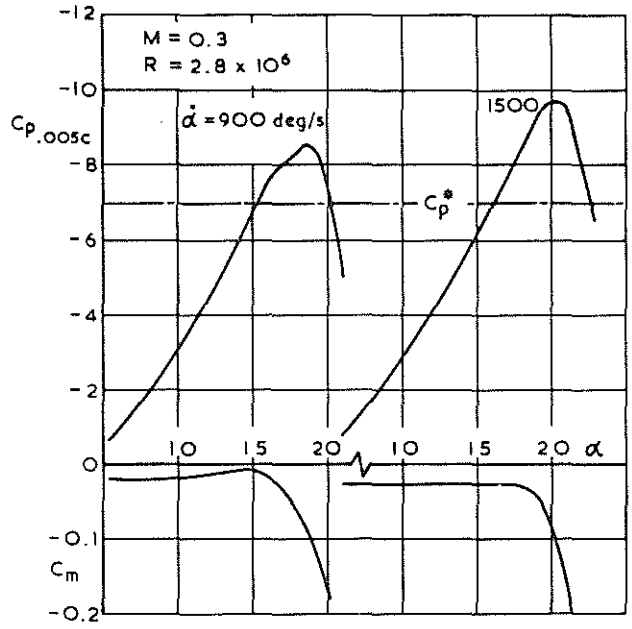

Fig 29 Variation of leading-edge pressure coefficient and pitching-moment coefficient with incidence during steady pitch rate motion for RAE 9681

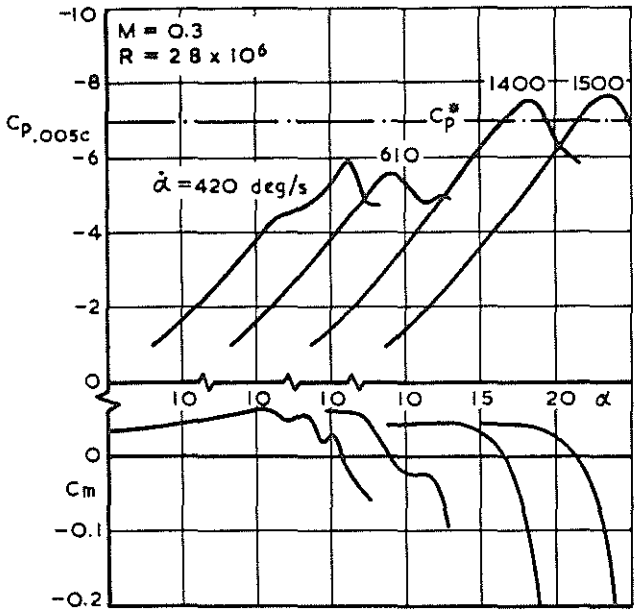

Fig 30 Variation of leading-edge pressure coefficient and pitching-moment coefficient with incidence during steady pitch rate motion for RAE 9651

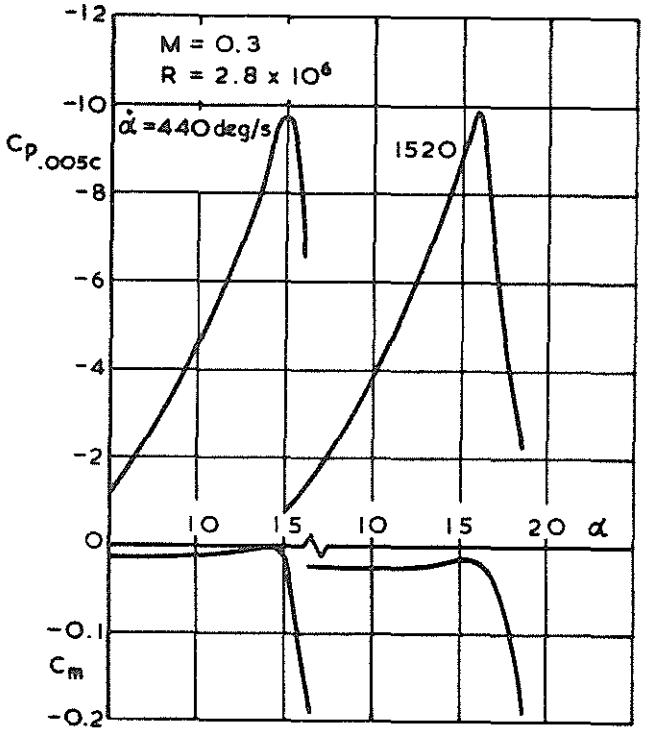

Fig 31 Variation of leading-edge pressure coefficient and pitching-moment coefficient with incidence during steady pitch rate motion for RAE 9634

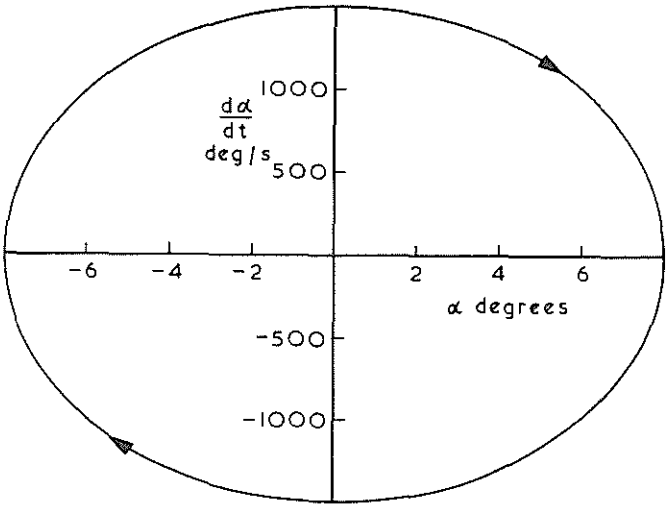

Fig 32 Variation of pitch rate with incidence during sinusoidal pitch oscillation at 30 Hz